G Protein-Bound Conformation of Mastoparan-X: Heteronuclear Multidimensional Transferred Nuclear Overhauser Effect Analysis of Peptide Uniformly Enriched with ^{13}C and ^{15}N[†,‡]

Hideki Kusunoki,[§,||] Kaori Wakamatsu,[||,⊥] Kazuki Sato,[§] Tatsuo Miyazawa,[#,△] and Toshiyuki Kohno*[,§]

Mitsubishi Kasei Institute of Life Sciences, Minamiooya, Machida-shi, Tokyo 194, Japan, Department of Biochemical Sciences, Faculty of Engineering, Gunma University, Kiryu, Gunma 376, Japan, The Institute of Physical and Chemical Research (RIKEN), Wako, Saitama 351-01, Japan, and Protein Engineering Research Institute, Furuedai, Suita, Osaka 565, Japan

Received November 7, 1997; Revised Manuscript Received January 5, 1998

ABSTRACT: Mastoparans, a family of tetradecapeptides from wasp venom, have been used as convenient low molecular weight models of receptors coupled to GTP-binding regulatory proteins (G proteins) for the understanding of the interaction between G proteins and receptors. Sukumar and Higashijima have analyzed the conformation of mastoparan-X (MP-X) bound to the G protein α-subunit using proton two-dimensional transferred nuclear Overhauser effect (TRNOE) spectroscopy [Sukumar, M., and Higashijima, T. (1992) *J. Biol. Chem., 267*, 21421−21424]. The resultant structure, however, was not well-defined due to severe overlap of peptide proton resonances. To determine the G protein-bound conformation of MP-X in detail, we have analyzed this interaction by heteronuclear multidimensional TRNOE experiments of MP-X uniformly enriched with ^{15}N and/or ^{13}C. By solving the overlap problem, we were able to determine the precise conformation of MP-X bound to Gi1α: the peptide adopts an amphiphilic α-helix from Trp3 to C-terminal Leu14, and the atomic root-mean-square deviation (rmsd) values in this portion about the averaged coordinates were 0.27 ± 0.07 Å for the backbone atoms (N, C^{α}, C′) and 0.84 ± 0.16 Å for all heavy atoms. These values are much smaller than the corresponding rmsd values of the structures obtained from the proton 2D TRNOE spectrum alone: 1.70 ± 0.41 Å for the backbone atoms (N, C^{α}, C′) and 2.84 ± 0.51 Å for all heavy atoms. Our results indicate that the heteronuclear multidimensional TRNOE experiments of peptides uniformly enriched with stable isotopes are a very powerful tool for analyzing the conformation of short peptides bound to large proteins. We will also discuss the structure−activity relationships of mastoparans in activating G proteins on the basis of the precise structure of MP-X bound to Gi1α.

Mastoparans [MPs,[1] Figure 1; reviewed by Nakajima et al. (*1*)], a family of tetradecapeptides from wasp venom, have been shown to directly activate GTP-binding regulatory proteins [G proteins, reviewed by Gilman (*2*)] in a manner similar to those of G protein-coupled receptors (*3*). (i) These peptides show selectivity among G proteins: they strongly activate Go and Gi but not Gs or Gt (*3*). (ii) ADP-ribosylation of G proteins (Gi and Go) by pertussis toxin inhibits the activation by MPs (*2, 4*). (iii) MP competes with receptors for binding to a common site on G proteins (*5*).

```
          1    5    10   14
MP        INLKALAALAKKIL-NH2
MP-X      INWKGIAAMAKKLL-NH2
MP-S      INWKGIASMURQVL-NH2
```

FIGURE 1: Amino acid sequences of MP, MP-X, and MP-S (U = α-aminoisobutyric acid).

MPs are thus particularly useful for analyzing G protein activation when employed as low molecular weight mimetics of receptors.

MPs show a striking conformational change in going from aqueous solution to lipid environments. Their CD spectra

† This work was supported in part by the Ministry of Education, Science, Sports and Culture, Japan, the Protein Engineering Research Institute, the Saneyoshi Foundation, the New Energy and Industrial Technology Development Organization (NEDO), and the Institute of Physical and Chemical Research (RIKEN).

‡ Atomic coordinates for the 14 converged structures of Mastoparan-X have been deposited with the Protein Data Bank, Brookhaven National Laboratories, Long Island, NY 11973, under the accession code 1a13.

* To whom correspondence should be addressed. Fax: +81(427)-24-6317. E-mail: tkohno@libra.ls.m-kagaku.co.jp.

§ Mitsubishi Kasei Institute of Life Sciences.

|| Gunma University.

⊥ The Institute of Physical and Chemical Research (RIKEN).

Protein Engineering Research Institute.

△ Deceased.

[1] Abbreviations: CD, circular dichroism; DSS, 4,4-dimethyl-4-silapentane-1-sulfonic acid; DTT, dithiothreitol; G protein, GTP-binding regulatory protein; GTPγS, guanosine 5′-*O*-(3-thiotriphosphate); Gi, a G protein that mediates inhibition of adenylyl cyclase; Gi1α, recombinant α-subunit of Gi; Go, an abundant G protein in brain; Gs, a G protein that mediates activation of adenylyl cyclase; Gt (transducin), an abundant G protein in retina; HMQC, heteronuclear multiple-quantum coherence; HSQC, heteronuclear single-quantum coherence; MP, mastoparan; MP-X, mastoparan-X; MPX-G, MP-X C-terminally flanked by a glycine residue; NMR, nuclear magnetic resonance; NOE, nuclear Overhauser effect; NOESY, NOE spectroscopy; rmsd, root-mean-square deviation; TOCSY, total correlation spectroscopy; TR-NOE, transferred NOE; WATERGATE, water suppression by gradient-tailored excitation; YUH, yeast ubiquitin hydrolase. Standard abbreviations are used for amino acids.

S0006-2960(97)02756-6 CCC: $15.00
Published on Web 03/18/1998

in water indicate the absence of an ordered structure, whereas those in the presence of phospholipid micelles or vesicles are characteristic of an α-helical conformation (*6*−*8*). It is known that the physiological activities of many peptides are correlated with their affinities to phospholipid membranes (*9, 10*). Also, activities of many peptides are better correlated to their conformations in the membrane-bound state than to those in an aqueous state (*7, 11, 12*). In fact, the activation of G protein by MPs is enhanced in the presence of phospholipid vesicles (*3*). Conformation analyses of MPs bound to G proteins as well as to phospholipid membranes are thus important to clarify the structure−activity relationships of MPs in activating G proteins.

We previously determined the membrane-bound conformation of mastoparan-X (MP-X, Figure 1) using the proton 2D transferred nuclear Overhauser effect (TRNOE, *13*−*16*) in the presence of perdeuterated phospholipid vesicles and found that the molecule adopts an amphiphilic α-helix from Trp3 to C-terminal Leu14 (*17*). The G protein-bound conformation of MP-X was similarly analyzed using the proton 2D TRNOE method in the presence of Gi1α protein by Sukumar and Higashijima (*18*). The structure obtained in their study was, however, too poorly defined to be compared with that bound to membranes, due to severe overlap of peptide proton resonances under the conditions employed (low temperature and relatively high pH). Hence, to elucidate the structure−activity relationships of MPs, it is still essential to determine the G protein-bound conformation of the peptides in more detail.

The TRNOE method has been widely used to determine conformations of peptides bound to large proteins or lipids (*17*−*21*). However, this method suffers from poor dispersion of peptide proton resonances since the peptide molecules in a free state, through which the information about the bound conformation is monitored, are primarily in a random coil state. In NMR analyses of proteins, the problem of poor proton resonance dispersion was alleviated by employing heteronuclear multidimensional NMR experiments using proteins uniformly enriched with stable isotopes, ^{13}C and ^{15}N (*22*). This strategy seems applicable also to "random coil" peptides since uniformly ^{13}C- or ^{15}N-enriched polypeptides in a urea-unfolded state gave well-dispersed signals in 2D $^{1}H-^{13}C$ or $^{1}H-^{15}N$ spectra (*23, 24*). Here we report the conformation analysis of MP-X bound to Gi1α by heteronuclear 3D TRNOE experiments of MP-X uniformly enriched with ^{15}N and/or ^{13}C, in conjunction with simulated annealing calculations. We will also discuss the structure−activity relationships of MPs on the basis of the precise structure of MP-X determined in this study.

MATERIALS AND METHODS

Preparation of MP-X. MP-X uniformly enriched with ^{15}N and/or ^{13}C was expressed in *Escherichia coli* cells and purified using a ubiquitin fusion protein system as described elsewhere (*68*). Briefly, MP-X C-terminally flanked by a glycine residue (MPX-G) was overexpressed in *E. coli* strain BL21(DE3) as a recombinant fusion protein with *Saccharomyces cerevisiae* ubiquitin under the control of the T7 promoter. The fusion protein contained a decahistidine tag at its N-terminus to facilitate subsequent purification via Ni^{2+}−NTA agarose affinity chromatography. The *E. coli* cells were grown in M9 minimal media containing $^{15}NH_4Cl$ and/or [$^{13}C_6$]glucose, and the protein was purified via Ni^{2+}−NTA agarose affinity chromatography. Yeast ubiquitin hydrolase (YUH), which specifically cleaves the ubiquitin fusion protein at the C-terminus of ubiquitin, was separately overexpressed in *E. coli* strain BL21(DE3) with a C-terminal hexahistidine tag using the T7 promoter and purified via Ni^{2+}−NTA agarose affinity chromatography. The ubiquitin−MPX-G was cleaved by YUH, the resultant MPX-G was purified by reversed-phase HPLC, and its C-terminal glycine residue was converted to an amide group by peptidylglycine α-amidating enzyme. The resultant MP-X uniformly enriched with ^{15}N and/or ^{13}C was purified again by HPLC and then pooled and lyophilized. Nonenriched MP-X was chemically synthesized by standard solid-phase methodology. The primary structure and purity of the peptide was confirmed by analytical HPLC, together with amino acid analysis.

NMR Sample Preparation. Acetic acid-d_4 (98%), DTT-d_{10} (98.4%), and D_2O (99.9%) were purchased from ISOTEC Inc. Nonenriched MP-X was chemically synthesized by standard solid-phase methodology. MP-X uniformly enriched with ^{15}N and/or ^{13}C was expressed in *E. coli* cells and purified using a ubiquitin fusion protein system as described above. The primary structure and purity of the peptide was confirmed by analytical HPLC, together with amino acid analysis. Peptides were dissolved in an NMR sample buffer [90% H_2O/10% D_2O or 99.9% D_2O containing 10 mM acetic acid-d_4 (pH 6.0) and 1 mM DTT-d_{10}]. The sample pH (direct pH meter reading) was adjusted to 6.1 ± 0.1. Recombinant polyhistidine-tagged Gi1α (Gi1α) was expressed in *E. coli* cells and purified using Ni^{2+}−NTA agarose and Mono Q chromatography according to reported procedures (*25*). The purity of the protein after Mono Q chromatography was confirmed by SDS−PAGE. They were exchanged into the NMR sample buffer (pH 6.0) by repetitive dilution and concentration using Centricon-10 ultrafiltration (Amicon). Protein concentrations were determined by amido black staining with BSA as the standard (*26*).

NMR Spectroscopy. All NMR measurements were performed on either a Bruker AMX-500 or ARX-400 spectrometers at 20 °C. The experiments are listed in Table 1. All proton 2D NMR spectra were acquired in a phase-sensitive mode using the time-proportional phase increments (TPPI) method (*27*) for quadrature detection in the t_1 dimension. All heteronuclear NMR spectra were acquired in a phase-sensitive mode using States−TPPI (*28*) for quadrature detection in the indirect dimensions.

Nonenriched MP-X was used to record 2D NOESY and TOCSY experiments. The water resonance was suppressed by coherent presaturation during the 1-s relaxation delay and during the NOESY mixing time τ_m. TOCSY spectra were recorded using a MLEV-17 pulse scheme (*29*) with a isotropic mixing time of 80 ms in the absence and presence of Gi1α. NOE spectroscopy (*30, 31*) in the absence of Gi1α was performed with a mixing time of 100 ms. NOESY spectra in the presence of Gi1α were performed with mixing times between 50 and 200 ms for checking the spin diffusion effect. The intensities of TRNOE cross peaks were found to be roughly linear up to 100 ms, suggesting that the spin diffusion effect is negligible in this range.

Table 1: Parameters for NMR Experiments

NMR experiment	nucleus			no. of points			final matrix size			spectral width (Hz)		
	F_1	F_2	F_3	F_1	F_2	F_3	F_1	F_2	F_3	F_1	F_2	F_3
nonenriched MP-X												
2D TOCSY	^{1}H	^{1}H		512	2048		1024	2048		6250	6250	
2D NOESY	^{1}H	^{1}H		512	2048		1024	2048		6250	6250	
^{15}N-enriched MP-X												
2D HSQC[c]	^{15}N	^{1}H		256	2048		256	1024[a]		1200	6250	
3D TOCSY−HSQC[c]	^{1}H	^{15}N	^{1}H	128	128	1024	256	256	512[a]	6250	1200	6250
3D NOESY−HSQC[c]	^{1}H	^{15}N	^{1}H	128	64	1024	256	256	512[a]	6250	1400	6250
3D HMQC−NOESY−HMQC[c]	^{15}N	^{15}N	^{1}H	64	64	1024		128	128	512[a]		6250
^{13}C- and ^{15}N-enriched MP-X												
2D HSQC[e]	^{13}C	^{1}H		256	2048		256	2048		20000	6250	
3D HNCO[c,h]	^{15}N	13C′	^{1}H	128	48	1024	256	256	512[a]	1200	1000	6250
3D HNCACB[d,f]	^{13}C	^{15}N	^{1}H	96	56	1024	256	256	512[a]	8000	1250	6250
3D CBCA(CO)NNH[d,f]	^{13}C	^{15}N	^{1}H	96	60	1024	256	256	512[a]	8000	1250	6250
3D TOCSY−HSQC[g]	^{1}H	^{13}C	^{1}H	80	32	1024	128	128	512[b]	6250	7400	6250

[a] The spectral data in this dimension were extracted only for the amide regions. [b] The spectral data in this dimension were extracted only for the aliphatic regions. [c] The ^{15}N carrier was palced at 119 ppm. [d] The ^{15}N carrier was placed at 118.6 ppm. [e] The ^{13}C carrier was placed at 86.7 ppm. [f] The ^{13}C carrier was placed at 45.4 ppm. [g] The ^{13}C carrier was placed at 35.7 ppm. [h] The ^{13}C′ carrier was placed at 176.5 ppm. The ^{1}H carrier was placed on the water resonance at 4.85 ppm.

Uniformly ^{15}N-enriched MP-X was used to record a 2D ^{1}H−^{15}N HSQC (*32*), a three-dimensional (3D) ^{15}N-edited TOCSY−HSQC with a 80-ms mixing time, a 3D ^{15}N-edited NOESY−HSQC (*33*) with a 100-ms mixing time, and a 3D ^{1}H,^{15}N-edited HMQC−NOESY−HMQC (*34*) with a 100-ms mixing time using the parameters in Table 1. For a 2D HSQC, a 3D TOCSY−HSQC, and a 3D NOESY−HSQC, the water resonance was suppressed by using the WATERGATE scheme (*35*) and water flip-back pulse (*36*). For a 3D HMQC−NOESY−HMQC, the water resonance was suppressed by coherent presaturation during the 1-s relaxation delay and during the NOESY mixing time τ_m. Decoupling of ^{15}N was achieved by WALTZ-16 modulation (*37*).

Uniformly ^{13}C- and ^{15}N-enriched MP-X was used to record a 2D ^{1}H−^{13}C HSQC, a 3D HNCO (*38*, *39*), a 3D HNCACB (*38*−*40*), a 3D CBCA(CO)NH (*38*, *39*, *41*), a 3D ^{13}C-edited TOCSY−HSQC with a 80-ms mixing time, and a 3D ^{13}C-edited NOESY−HMQC (*42*) with a 100-ms mixing time using the parameters listed in Table 1. The 3D ^{13}C-edited TOCSY−HSQC experiment was performed using the pulse sequence modified from the 3D ^{15}N-edited TOCSY−HSQC. For a 2D HSQC, a 3D HNCO, a 3D HNCACB, a 3D CBCA(CO)NH, and a 3D TOCSY−HSQC, the water resonance was suppressed by using the WATERGATE scheme and water flip-back. For a 3D NOESY−HMQC, the water resonance was suppressed by coherent presaturation during the 1-s relaxation delay and during the NOESY mixing time τ_m. Decoupling of ^{15}N and C′ was achieved by WALTZ-16 modulation (*37*). Decoupling of ^{13}C was achieved by GARP modulation (*43*).

Data processing was performed either on a Bruker X-32 UNIX workstation with UXNMR software or on a Silicon Graphics INDIGO2 workstation using the program package NMRDraw and NMRPipe (*44*). For proton 2D NMR data sets, a 60° phase-shifted sine-squared window function was used in both dimensions prior to Fourier transformation. Final matrix sizes were usually 1024 × 2048 real points in the F_1 and F_2 dimensions, respectively. For 3D heteronuclear NMR data sets, linear prediction methods (*45*, *46*) were employed to extend the data in the indirectly acquired dimensions. After linear prediction, a 72° phase-shifted sine-squared window function and a single zero-filling was used in all dimensions prior to Fourier transformation.

In all experiments, the ^{1}H carrier was placed on the H_2O resonance at 4.85 ppm, both ^{15}N and ^{13}C carriers were set differentially, respectively, depending on the experiments, as shown in Table 1. All proton chemical shifts were referenced to the methyl resonance of 4,4-dimethyl-4-silapentane-1-sulfonic acid (DSS) used as an internal standard. The ^{13}C and ^{15}N chemical shifts were indirectly referenced using the following ratios of the zero-point frequencies: 0.101 329 118 for ^{15}N to ^{1}H and 0.251 449 53 for ^{13}C to ^{1}H (*47*).

GTPγS Binding Assay. The activation of Gi1α by MP-X was examined as a function of pH using the [^{35}S]GTPγS binding assay as described previously (*3*, *48*). The enhancement of [^{35}S]GTPγS binding to Gi1α by MP-X showed that the enhancing activities at pH 6.0 and 8.0 were almost identical. This is consistent with previous data obtained from MP-X-stimulated GTPase activity (*18*). The stability of Gi1α during NMR experiments was confirmed by [^{35}S]-GTPγS binding activity (*48*): the protein kept 60−70% of the original activity for 42 h under the conditions of the NMR experiments, indicating that the observed TRNOEs reflect interaction of MP-X with intact Gi1α.

Distance Constraints and Structure Calculations. Interproton distance restraints were obtained from the homonuclear and heteronuclear NOESY spectra with a mixing time of 100 ms. Quantitative determination of cross-peak intensities was based on counting the contour levels, where the 4H−5H crosspeak of Trp3 was chosen as the standard with a distance of 2.5 Å. All NOE data were divided into three classes, strong, medium, and weak, corresponding to distance upper limits of 2.7, 3.6, and 4.5 Å in the interproton distance restraints. Pseudoatoms were used for nonstereospecifically assigned protons, and intraresidue correcting factors were added to the distance restraints (*49*). In addition, 0.5 Å was added to the upper limits for distance restraints involving methyl protons (*50*).

All calculations were carried out on a HP 9000/720 workstation with the X-PLOR 3.1 program (*51*). The three-dimensional structures were calculated on the basis of the

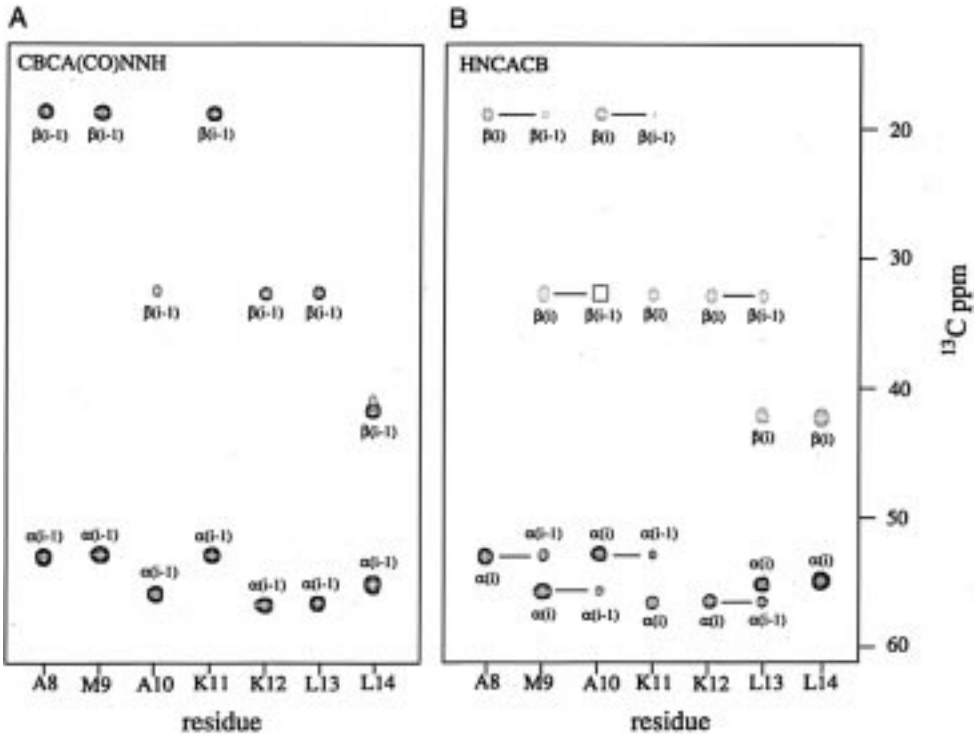

FIGURE 2: Strips extracted from CBCA(CO)NH (A) and HNCACB (B) spectra, showing connectivities of residues A8−L14. Red contours indicate negative peaks. Horizontal solid lines indicate sequential C^{α} and C^{β} connectivities. The square indicates the $^{13}C^{\beta}$ resonances of M9.

experimentally derived distance constraints using a dynamically simulated annealing protocol starting from a template structure with randomized backbone ϕ and ψ torsion angles.

Evaluation Methods. The convergence of the calculated structures was evaluated in terms of the structural parameters, i.e., rms deviations from experimental distance and dihedral constraints, the values of energetic statistics (F_{NOE} and F_{repel}), and rms deviations from idealized geometry. The distribution of backbone dihedral angles of the final converged structures was evaluated by the representation of the Ramachandran dihedral pattern, indicating the deviations from the sterically allowed (ϕ, ψ) angle limits (*52*). The degree of angular variation among the converged structures was further assessed by using an angular order parameter *S* (*53*). The order parameter *S* was calculated by using the equation:

$$S = \frac{1}{N}[(\sum_{j=1}^{N} \sin\theta_j)^2 + (\sum_{j=1}^{N} \cos\theta_j)^2]^{1/2}$$

N is the number of total converged structures and θ_j is a particular dihedral angle of the *j*th structure of the total structures.

RESULTS

TRNOEs. On addition of Gi1α, peptide resonances were uniformly broadened without any detectable chemical shift changes in a proton 1D NMR spectrum (data not shown), suggesting that MP-X in the free state is in slow chemical exchange with MP-X in the Gi1α-bound state. We carried out all TRNOE experiments at a protein:peptide ratio of 1:20 (5 mM MP-X) because this concentration ratio gives TRNOE cross peaks of sufficient intensity without broadening them too much. In a NOESY spectrum of MP-X alone (τ_m = 100 ms), only a few weak NOEs were observed, being

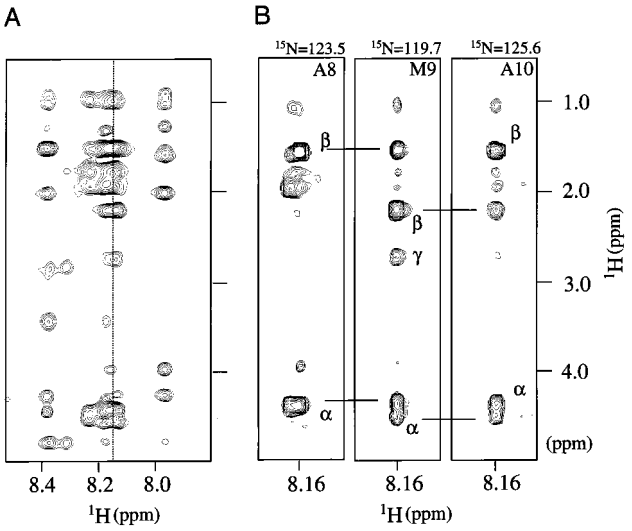

FIGURE 3: TRNOE spectra of the MP-X (5 mM) in the presence of Gi1α (0.25 mM) at pH 6.0 and 20 °C. (A) Amide−aliphatic fingerprint region of a proton 2D TRNOE spectrum. The amide proton chemical shifts of residues Ala8−Ala10 are indicated by a vertical dotted line. (B) Three strips of the ^{15}N-edited TRNOE spectra for the ^{15}N chemical shift of residues Ala8−Ala10. Horizontal solid lines indicate sequential $d_{\alpha N}$ and $d_{\beta N}$ connectivities.

consistent with the expectation that the magnitude of NOEs is close to zero for small peptides such as MP-X. In contrast, a TRNOESY spectrum of MP-X in the presence of Gi1α showed many strong negative NOEs (Figure 3A) as reported previously (*18*). These observations indicate that these NOEs reflect the conformation of MP-X molecules in the G protein-bound state. It should be noted that the observed NOEs in the presence of Gi1α are due to specific interaction of MP-X and Gi1α because it is known that BSA, which binds many kinds of small molecules, failed to give a similar NOE pattern

and that no TRNOEs were observed in the presence of heat-denatured G protein (*18*).

Resonance Assignments of MP-X. Figure 3A shows the amide−aliphatic fingerprint region of a proton 2D NOESY spectrum of MP-X in the presence of Gi1α. Resonance assignments based on sequential α_i-N_{i+1} NOE cross peaks could not be carried out unambiguously because of severe overlap of amide and C^α proton resonances: seven resonances in 8.16−8.20 ppm and five in 4.23−4.25 ppm, respectively. We thus carried out heteronuclear 3D NMR experiments of uniformly ^{15}N- and ^{13}C-enriched MP-X. The assignments of the backbone resonances ($^{13}C^\alpha$, ^{15}N, NH) and $^{13}C^\beta$ resonances were obtained from the CBCA(CO)NH experiment, which correlates backbone ^{15}N and NH resonances with $^{13}C^\alpha$ and $^{13}C^\beta$ resonances of the preceding residue, and the HNCACB experiment, which correlates the $^{13}C^\alpha$ and $^{13}C^\beta$ resonances of the preceding residue with intraresidue backbone ^{15}N, NH, $^{13}C^\alpha$, and $^{13}C^\beta$ resonances. Figure 2 shows the sequence strips of the C-terminal half of MP-X taken from both the CBCA(CO)NH and HNCACB spectra. In this region of MP-X both spectra show excellent chemical shift dispersion due to well-dispersed signals in the ^{15}N dimension, although the proton NMR spectra show poor chemical shift dispersion. Both spectra shown in panels A and B of Figure 2 were very useful in order to complete the backbone assignments. Carbonyl carbon resonances were assigned by a 3D HNCO spectrum (data not shown). The assignments of side chain proton resonances were obtained from a 3D ^{15}N-edited TOCSY−HSQC spectrum of ^{15}N-enriched MP-X (data not shown). The assignments for side-chain carbon resonances were obtained from 3D ^{13}C-edited TOCSY−HSQC and 2D $^1H-^{13}C$ HSQC spectra of ^{13}C- and ^{15}N-enriched MP-X (not shown). Chemical shifts obtained are listed in Supporting Information. Details of ^{13}C and ^{15}N chemical shift resolutions in a random coil state will be reported elsewhere (*68*).

Assignment of NOEs. Figure 3B shows the amide−aliphatic fingerprint regions of slices taken from the 3D ^{15}N-edited TRNOE spectrum in the presence of Gi1α. For comparison, the corresponding region of a proton 2D TRNOESY spectrum is shown in Figure 3A. In Figure 3A, chemical shift degeneracy of amide protons prevented unambiguous identification of each NOE cross peak, especially those involving Ala8 through Ala10. However, these cross peaks were distinctly resolved in the 3D ^{15}N-edited TRNOE spectra (Figure 3B). The connectivities of αN(i,i+1) and βN(i,i+1) from Ala8 to Ala10 could be identified only by these spectra. Similarly, sequential NN(i,i+1) connectivities from Ala8 to Leu13 were identified unambiguously only from a 3D HMQC−TRNOESY−HMQC spectrum (data not shown). Furthermore, the ^{15}N-edited spectra showed NOE cross peaks characteristic of an α-helical conformation, αN(i,i+2), NN(i,i+2), and NN(i,i+3). NOE cross peaks in the aliphatic region, which are also severely overlapped in the proton 2D spectrum, were unambiguously assigned in a ^{13}C-edited TRNOE spectrum. The αβ(i,i+3) connectivities characteristic of an α-helical conformation were thus identified for pairs Ala8−Lys11 and Ala10−Leu13. Taken together, from heteronucleus-edited TRNOE spectra we could newly identify 23 interresidue and 12 intraresidue NOE cross peaks. Sequential and medium-range NOEs observed in the proton 2D and heteronuclear 3D TRNOESY spectra are summarized in Figure 4. NOE patterns characteristic of an α-helical conformation were apparent for Trp3 through C-terminal Leu14 from NN(i,i+1), αN(i,i+3), and αβ(i,i+3) NOEs.

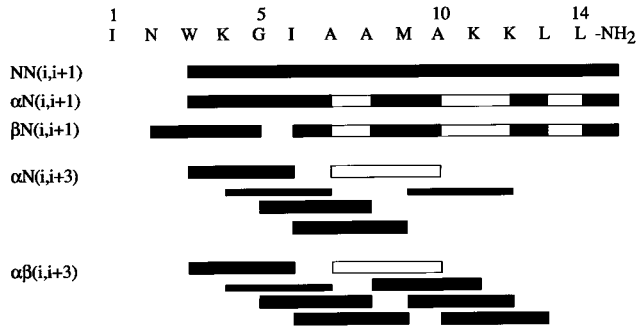

FIGURE 4: Summary of the NOE connectivities observed in MP-X bound to Gi1α. This structural information was used for the sequence-specific assignments and the identification of secondary structure elements in MP-X. Unambiguously identified NOE connectivities are indicated by filled bars spanning the residues involved in each NOE. Open bars represent NOEs which might be present but cannot be identified because of overlap of the resonances involved. The NOEs are classified into medium and weak according to the height of the filled bars.

Structure Calculations and Evaluation. To determine the detailed conformation of MP-X bound to Gi1α, we carried out structure calculations by X-PLOR with simulated annealing protocols using 151 distance constraints [74 intraresidue and 77 interresidue: 28 sequential ($|i-j|=1$) and 49 medium range ($1<|i-j|\leq 4$), Figure 5A] obtained from homonuclear 2D and heteronuclear 3D TRNOE spectra. Simulated annealing calculations were started from 100 random initial structures. We selected the 14 final structures with the lowest energies (<30 kcal/mol), for which none of the NOE distance violation was larger than 0.5 Å. In these 14 structures, there were only two violations larger than 0.2 Å (both 0.21 Å). Structural statistics for the mean and converged structures for MP-X were evaluated in terms of structural parameters, as shown in Table 2. The convergence was further assessed by the (ϕ, ψ) spacing for all selected structures. In a Ramachandran-type plot (Figure 6), most of the backbone dihedral angles of the final converged structures fall in the α-helical region.

The overall convergence of the final set of structures can be quantified by an atomic rmsd value. The rms deviations from the averaged coordinate positions were 0.84 ± 0.16 Å for the backbone atoms (N, C^α, C′) and 1.43 ± 0.12 Å for all heavy atoms. For the same atom selection, the average pairwise rmsd values of the 14 individual structures were 1.20 ± 0.39 and 2.08 ± 0.35 Å, respectively (Table 3).

Panels B and C of Figure 5 show the distribution of the atomic rmsd for the 14 converged structures fitted over the backbone heavy atoms (N, C^α, C′, O) of residues Trp3−Leu14 of the mean structure as a function of the residue number. The backbone structure is well-defined throughout this portion of the molecule. This is supported by small rmsd values of the Trp3−Leu14 region: these values from the averaged coordinate positions were 0.27 ± 0.07 Å for the backbone atoms (N, C^α, C′) and 0.93 ± 0.14 Å for all heavy atoms. For the same atom selection, the average pairwise rmsd values were 0.40 ± 0.11 and 1.37 ± 0.22 Å, respectively (Table 3).

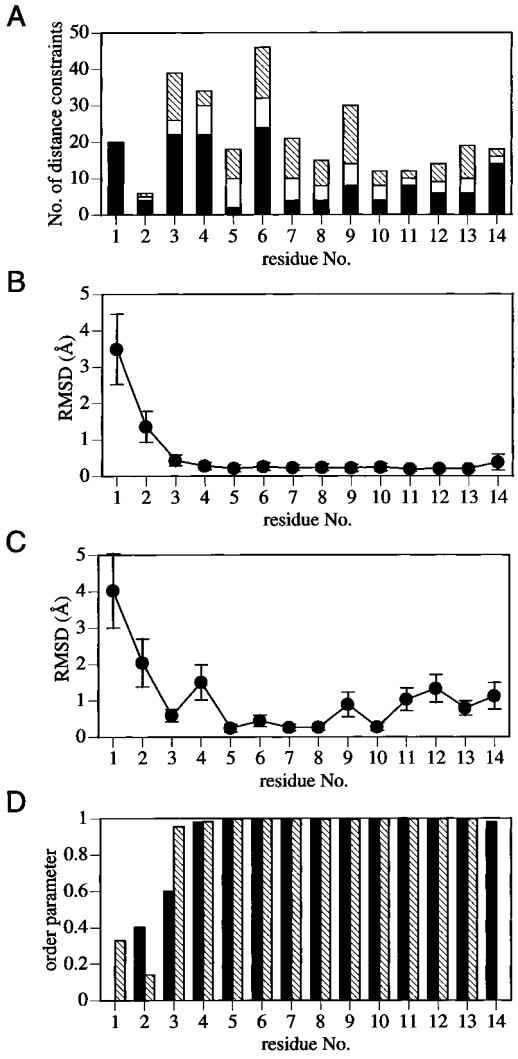

FIGURE 5: The number of NOE constraints and conformational convergence of each residue of Gi1α-bound MP-X. (A) Distribution of the number of experimental distance constraints as a function of the sequence position of MP-X. Key: filled bars, intraresidue NOEs; open bars, sequential NOEs; hatched bars, medium-range NOEs. (B and C) Distribution of the rms distance of the backbone (B) and all heavy atoms (C) from the mean structure as a function of residue number shown together with the standard deviations in these values. (D) Order parameter *S* of ϕ (filled bars) and ψ (hatched bars): 0 = randomly distributed and 1 = perfectly aligned.

Description of the Structure. Figure 7A shows the best-fit superposition of the backbone heavy atoms (N, C^{α}, C′) of Trp3−Leu14 for the 14 converged structures of MP-X bound to Gi1α. As expected from the NOE pattern shown in Figure 4, the peptide backbone from Trp3 to Leu14 is well-defined and adopts an amphiphilic α-helical conformation, with the three lysine side chains located on one side and the hydrophobic side chains located on the other side of the amphiphilic α-helix. The portion of the N-terminal two residues, Ile1 and Asn2, is rather disordered. The disorder in this region agrees well with its smaller order parameter value *S* (Figure 5D).

DISCUSSION

Structure of MP-X Obtained from Proton 2D TRNOE Analysis. In the present study, we have precisely determined the conformation of MP-X bound to Gi1α by the heteronuclear TRNOE experiments of peptides uniformly enriched with ^{15}N and/or ^{13}C. To demonstrate the impact of heteronuclear 3D TRNOE experiments, structural calculation was carried out using 116 distance constraints [62 intraresidue and 54 interresidue: 17 sequential ($|i - j| = 1$) and 37 medium range ($1 < |i - j| \leq 4$)] obtained from our proton 2D TRNOE experiment alone. The structural calculation was carried out using the same procedure as previously mentioned (see Results). Figure 7B shows 14 such structures fitted as those in Figure 7A. These structures are poorly defined and their rms deviations from the averaged coordinate positions are as large as 1.70 ± 0.41 Å for the backbone atoms (N, C^{α}, C′) and 2.84 ± 0.51 Å for all heavy atoms (Table 3).

Use of Peptides Uniformly Enriched with Stable Isotopes. Although the TRNOE method is useful for determining conformations of peptides bound to large proteins (*19*−*21*),

Table 2: Structural Statistics for MP-X[a]

structural parameter	14 converged structures	mean structure
rmsd from exptl distance constraints (Å)		
all (151)	0.028 ± 0.002	0.022
intraresidue (74)	0.021 ± 0.001	0.021
sequential ($\|i - j\| = 1$) (28)	0.012 ± 0.003	0.018
medium range ($1 < \|i - j\| \leq 4$) (49)	0.041 ± 0.005	0.027
energetic statistics (kcal mol^{-1})[b]		
F_{NOE}	6.20 ± 0.99	3.9
F_{repel}	4.95 ± 1.31	2.7
E_{L-J}	−17.2 ± 6.8	−18.2
rmsd from idealized geometry		
bonds (Å)	0.002 ± 0.0002	0.002
angles (deg)	0.338 ± 0.024	0.290
impropers (deg)	0.318 ± 0.033	0.269

[a]The 14 converged structures refer to the final set of dynamical simulated annealing structures starting from 100 initial random structures; the mean structure was obtained by restrained minimization of the averaged coordinates of the 14 individual structures. The number of each experimental constraint used in the calculations is given in parentheses. [b] F_{NOE} and F_{repel} are the energies related to the NOE violations, the torsion angle violations, and the van der Waals repulsion term, respectively. The values of the force constants used for these terms are the standard values as implemented in the X-PLOR 3.1 manual (*51*). E_{L-J} is the Lennard-Jones van der Waals energy calculated with the CHARMm (*52*) empirical energy function.

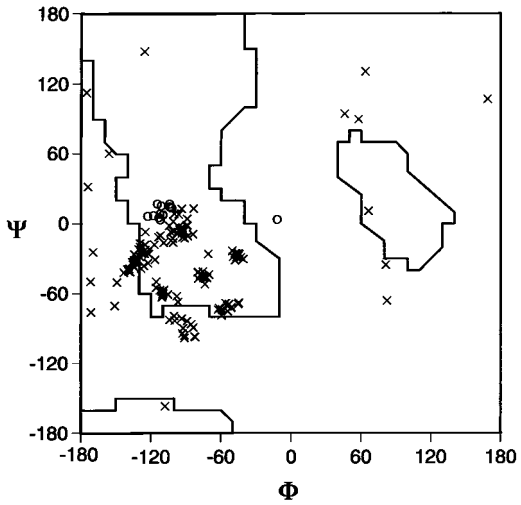

FIGURE 6: Ramachandran plots of the backbone conformational (ϕ, ψ) angles for all residues of the converged structures of MP-X bound to Gi1α. Circles (○) indicate the glycine residue at the fifth position and the crosses (×) indicate other residues.

Table 3: Comparison of rmsd Value between Uniformly ^{13}C- and ^{15}N-Enriched and Nonenriched MP-X[a]

	atomic rmsd of 14 converged structures vs mean structure (Å)		av pairwise rmsd of 14 converged structures (Å)	
	residues 1−14	residues 3−14	residues 1−14	residues 3−14
Heteronuclear TRNOE Analysis of Uniformly ^{13}C- and ^{15}N-Enriched MP-X				
backbone				
N, C[a], C′	0.84 ± 0.16	0.27 ± 0.07	1.20 ± 0.39	0.40 ± 0.11
N, C[a], C′, O	0.85 ± 0.13	0.31 ± 0.09	1.21 ± 0.33	0.46 ± 0.13
all heavy atoms	1.43 ± 0.12	0.93 ± 0.14	2.08 ± 0.28	1.37 ± 0.22
Homonuclear TRNOE Analysis Alone of Nonenriched MP-X				
backbone				
N, C[a], C′	1.93 ± 0.31	1.70 ± 0.41	2.73 ± 0.74	2.34 ± 0.84
N, C[a], C′, O	2.01 ± 0.31	1.81 ± 0.41	2.85 ± 0.73	2.51 ± 0.84
all heavy atoms	3.05 ± 0.39	2.84 ± 0.51	4.32 ± 1.01	3.95 ± 1.18

[a] The rmsd values were obtained by best fitting the backbone atom (N, C[a], C′, O) coordinates for all residues of the 14 converged structures. The numbers given for the backbone and all heavy atoms represent the mean values ± standard deviations.

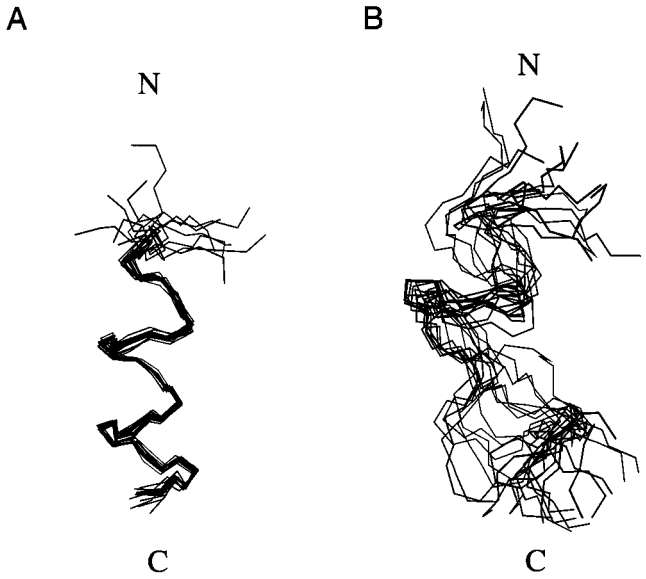

FIGURE 7: Backbone structures (N, C^{α}, C′) of the 14 converged structures of MP-X bound to Gi1α (A) obtained from heteronuclear 3D TRNOE experiments and (B) obtained from proton 2D TRNOE experiments alone. Structures are the best fit of the backbone heavy atoms (N, C^{α}, C′) of residues Trp3−Leu14. The figure was prepared using MIDAS Plus (*66*).

it does have a few drawbacks: (i) There is poor signal dispersion of peptide proton resonances, especially under the conditions of low temperature and relatively high pH. (ii) Dihedral constraints cannot be used in structural determination. To determine precise conformations of peptides bound to large proteins, as many NOEs as possible need to be observed in the TRNOE spectra by solving the overlap problem. In such a case, a $^{1}H-^{15}N$ TRNOE experiment with selectively ^{15}N-enriched peptides has been used as a way to resolve this problem (*55, 56*). However, the heteronuclear TRNOE strategy with uniformly enriched peptides has not yet been widely used probably for the following reasons: Uniformly enriched peptides are too expensive to be synthesized chemically, and a procedure needed to express and enrich short peptides with stable isotopes in *E. coli* cells is much more complex than the one used for proteins. Thus,

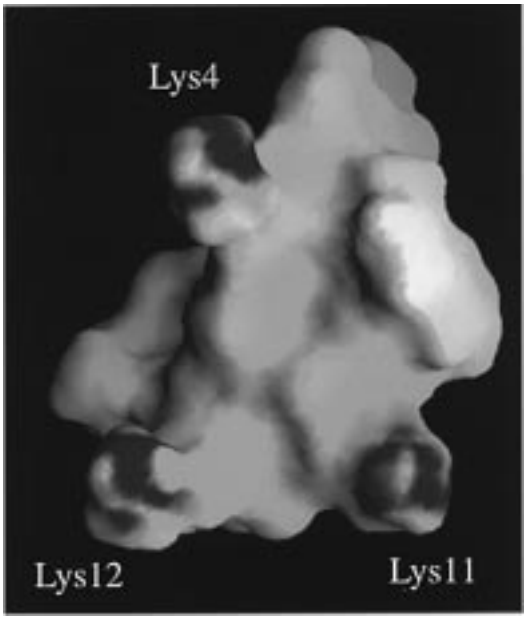

FIGURE 8: Electrostatic potential representations of MP-X bound to Gi1α. Blue regions represent positive potentials of lysine residues. White regions represent neutral potentials. The figure was prepared using the program GRASP (*67*).

in this study we employed a new general method to prepare isotope-enriched peptides that uses a ubiquitin fusion system. In fact, we could prepare MP-X uniformly enriched with ^{15}N and/or ^{13}C in 2 weeks. The heteronuclear 3D TRNOE experiments of such peptides provide invaluable information which enabled determination of MP-X conformation bound to G protein in detail as shown in Figure 7A, even when the dihedral constraints cannot be used in structural calculation.

Structure−Activity Relationships of MP-X. The Gi-bound MP-X molecules adopt an amphiphilic α-helix from Trp3 to C-terminal Leu14 with three lysine side chains located on one side of the helix and hydrophobic side chains on the opposite side. The N-terminal two residues, Ile1 and Asn2, are not well-defined. This MP-X structure is similar to the one in the membrane-bound state (*17*). Such a similarity has been predicted on the basis of the observation that the activation of G proteins by MPs is much more pronounced when G proteins are reconstituted in phospholipid vesicles than in a detergent solution (*3*). Moreover, this similarity suggests that the amphiphilic α-helix structure of MPs may be important in activating G proteins. This is also supported by a previous observation that the extent of activation of G proteins by MPs decreases when they are designed to have low amphiphilic moments (*5*).

Structure−activity relationship studies of MPs have shown that positive charges are crucial for regulatory activity on G proteins (*5*). The three lysine residues at the 4th, 11th, and 12th positions are conserved in MPs isolated from wasp venom (*1*). Thus, it is likely that the positive charges are placed on one face to facilitate the binding interaction with G proteins. Figure 8 shows the hydrophilic surface of the amphiphilic α-helix of the average structure of MP-X. The three lysine residues, Lys4, Lys11, and Lys12, are placed on one side of the helix, and the side chains of these extend in the same direction. This is in good agreement with the structure−activity relationships of MPs in activating G proteins.

Similarities between Mastoparans and G Protein-Coupled Receptors. Studies of site-directed mutagenesis, chimera, and synthetic peptides of G protein-coupled receptors have suggested that the N- and C-terminal parts of the third inner loop and the N-terminal part of the C-terminal tail as well as the second inner loop are all important for the activation of G proteins (*57*−*59*). Recently, Wess and co-workers (*60*−*62*) have reported that the C-terminal part of the third inner loop of m2 muscarinic receptor can specifically recognize the C-terminus of α-subunits of Gi/o, leading to G protein activation. Secondary structure prediction (*63*) and a recent mutagenesis study (*64*) suggest that this region of m2 muscarinic receptor is α-helically arranged, with the positively charged residues located on one side and with the hydrophobic residues located on the opposite side. This predicted secondary structure is similar to the conformation of Gi1α-bound MP-X elucidated in the present study. It has been reported that MP binds the C-terminal region of Giα (*65*) and MP inhibits the ability of Go to increase the affinity of agonists binding to the m2 muscarinic receptor (*5*). Taking these observations into account, the C-terminal part of the third inner loop of m2 receptors is expected to take a conformation similar to that of Gi-bound MP-X determined in this study.

Comparison of the Structure of Gi-Bound MP-X and Gs-Bound MP-S. Very recently, Sukumar and co-workers determined by proton 2D TRNOE experiments the Gs-bound conformation of MP-S (Figure 1), one of a few mastoparan analogues that can activate Gs (*21*). Their data indicated that MP-S molecules adopt an α-helical conformation with a kink at residue 9 when bound to Gs as well as to Gi or Go. They suggested that a kinked helix is optimal for activating Gs, whereas a straight helix is the optimal conformation for activating Gi/o. However, they also described that it is difficult to clearly correlate differential specificities of MP-S and MP-X with their different G protein-bound conformations because the Gi/o-bound conformations that they determined are poorly defined. The Gi-bound conformation of MP-X precisely determined in this study is a straight α-helix in the portion from Trp3 to C-terminal Leu14. Although our data support their postulation, we would like to suggest that the postulation can be more rigorously examined when the Gs-bound conformation of MP-S is analyzed by our present strategy.

In conclusion, we have demonstrated that the heteronuclear multidimensional TRNOE experiments of peptides uniformly enriched with ^{13}C and ^{15}N are powerful in determining detailed conformations of peptides bound to large proteins. We believe that our present study will be useful for the development of peptides that specifically regulate G proteins and for the understanding of receptor−G protein interactions.

ACKNOWLEDGMENT

We thank Dr. Frank Delaglio at the NIH for providing us with the NMRPipe/NMRDraw software, Dr. Yutaka Ito at The Institute of Physical and Chemical Research (RIKEN) for providing us with pulse sequences, Dr. Akira Omori and Mrs. Sachiyo Ichinose for amino acid sequencing of mastoparan-X, and Ms. Kuniko Kobayashi for her help in structural calculation at the Mitsubishi Kasei Institute of Life Sciences. We also thank Drs. Takao Matsuzaki at the Mitsubishi Kasei Institute of Life Sciences and Yoshio Kodera at the Department of Physics, Kitasato University, for helpful discussion, as well as Dr. Arno Pähler at Mitsubishi Chemical Inc. for critical reading of the manuscript.

SUPPORTING INFORMATION AVAILABLE

One table containing NMR chemical shifts of ^{1}H, ^{15}N, $^{13}C'$, and ^{13}C resonances of MP-X (1 page). Ordering information is given on any current masthead page.

REFERENCES

1. Nakajima, T., Uzu, S., Wakamatsu, K., Saito, K., Miyazawa, T., and Yasuhara, T. (1986) *Biopolymers 25*, S115−S121.
2. Gilman, A. G. (1987) *Annu. Rev. Biochem. 56*, 615−649.
3. Higashijima, T., Uzu, S., Nakajima, T., and Ross, E. M. (1988) *J. Biol. Chem. 263*, 6491−6494.
4. Higashijima, T., Uzu, S., Nakajima, T., and Miyazawa, T. (1987) *in Peptide Chemistry 1986* (Miyazawa, T., Ed.) pp 75−78, Protein Research Foundation, Osaka, Japan.
5. Higashijima, T., Burnier, J., and Ross, E. M. (1990) *J. Biol. Chem. 265*, 14176−14186.
6. Wakamatsu, K., Higashijima, T., Fujino, M., Nakajima, T., and Miyazawa, T. (1983) *FEBS Lett. 162*, 123−126.
7. Higashijima, T., Wakamatsu, K., Takemitsu, M., Fujino, M., Nakajima, T., and Miyazawa, T. (1983) *FEBS Lett. 152*, 227−230.
8. Higashijima, T., Wakamatsu, K., Saito, K., Fujino, M., Nakajima, T., and Miyazawa, T. (1984) *Biochim. Biophys. Acta 802*, 157−161.
9. Gysin, B., and Schwyzer, R. (1983) *FEBS Lett. 158*, 12−16.
10. Schwyzer, R. (1987) in *Peptides 1986* (Theodoropoulos, D., Ed.) pp 7−23, Walter de Gruyter, Berlin.
11. Jelicks, L. A., Broido., M. S., Becker, J. M., and Naider, F. R. (1989) *Biochemistry 28*, 4233−4240.
12. Milon, A., Miyazawa, T., and Higashijima, T. (1990) *Biochemistry 29*, 65−75.
13. Clore, G. M., and Gronenborn, A. M. (1982) *J. Magn. Reson. 48*, 402−417.
14. Clore, G. M., and Gronenborn, A. M. (1983) *J. Magn. Reson. 53*, 423−442.
15. Campbell, A. P., and Sykes, B. D. (1991) *J. Magn. Reson. 93*, 77−92.
16. Campbell, A. P., and Sykes, B. D. (1993) *Annu. Rev. Biophys. Biomol. Struct. 22*, 99−122.
17. Wakamatsu, K., Okada, A., Miyazawa, T., Ohya, M., and Higashijima, T. (1992) *Biochemistry 31*, 5654−5660.
18. Sukumar, M., and Higashijima, T. (1992) *J. Biol. Chem. 267*, 21421−21424.
19. Scherf, T., Hiller, R., Naider, F., Levitt, M., and Anglister, J. (1992) *Biochemistry 31*, 6884−6897.
20. Ni, F., Konishi, Y., and Scheraga, H. A. (1990) *Biochemistry 29*, 4479−4489.
21. Sukumar, M., Ross, E. M., and Higashijima, T. (1997) *Biochemistry 36*, 3632−3639.
22. Bax, A., and Grzesiek, S. (1993) *Acc. Chem. Res. 26*, 131−138.
23. Neri, D., Wider, G., and Wüthrich, K. (1992) *Proc. Natl. Acad. Sci. U.S.A. 89*, 4397−4401.
24. Neri, D., Wider, G., and Wüthrich, K. (1992) *FEBS Lett. 303*, 129−135.
25. Lee, E., Linder, M. E., and Gilman, A. G. (1994) *Methods Enzymol. 237*, 146−164.
26. Schaffner, W., and Weissmann, C. (1973) *Anal. Biochem. 56*, 502−514.
27. Marion, D., and Wüthrich, K. (1983) *Biochem. Biophys. Res. Commun. 113*, 967−974.
28. Marion, D., Ikura, M., Tschudin, R., and Bax, A. (1989) *J. Magn. Reson. 85*, 393−399.
29. Bax, A., and Davis, D. G. (1985) *J. Magn. Reson. 65*, 355−359.

30. Jeener, J., Meier, B. H., Bachmann, P., and Ernst, R. R. (1979) *J. Chem. Phys. 71*, 4546−4553.
31. Macura, S., Huang, Y., Suter, D., and Ernst, R. R. (1981) *J. Magn. Reson. 43*, 259−281.
32. Bodenhausen, G., and Ruben, D. J. (1980) *Chem. Phys. Lett. 69*, 185−189.
33. Jahnke, W., Baur, M., Gemmecker, G., and Kessler, H. (1995) *J. Magn. Reson. B 106*, 86−88.
34. Ikura, M., Bax, A., Clore, G. M., and Gronenborn, A. M. (1990) *J. Am. Chem. Soc. 112*, 9020−9022.
35. Piotto, M., Saudek, V., and Sklenár, V. (1992) *J. Biomol. NMR 2*, 661−665.
36. Grzesiek, S., and Bax, A. (1993) *J. Am. Chem. Soc. 115*, 12593−12594.
37. Shaka, A. J., Keeler, J., and Freeman, R. (1983) *J. Magn. Reson. 53*, 313−340.
38. Muhandiram, D. R., and Kay, L. E. (1994) *J. Magn. Reson. B 103*, 203−216.
39. Kay, L. E., Ikura, M., Tschudin, R., and Bax, A. (1990) *J. Magn. Reson. 89*, 496−514.
40. Wittekind, M., and Mueller, L. (1993) *J. Magn. Reson. B 101*, 201−205.
41. Grzesiek, S., and Bax, A. (1992) *J. Am. Chem. Soc. 114*, 6291−6293.
42. Ikura, M., Kay, L. E., Tschudin, R., and Bax, A. (1990) *J. Magn. Reson. 86*, 204−209.
43. Shaka, A. J., Barker, P. B., and Freeman, R. (1985) *J. Magn. Reson. 64*, 547−552.
44. Delaglio, F., Grzesiek, S., Vuister, G. W., Zhu, G., Pfeifer, J., and Bax, A. (1995) *J. Biomol. NMR 6*, 277−293.
45. Zhu, G., and Bax, A. (1990) *J. Magn. Reson. 90*, 405−410.
46. Zhu, G., and Bax, A. (1992) *J. Magn. Reson. 100*, 202−207.
47. Wishart, D. S., Bigam, C. G., Yao, J., Abildgaard, F., Dyson, H. J., Oldfield, E., Markley, J. L., and Sykes, B. D. (1995) *J. Biomol. NMR 6*, 135−140.
48. Northup, J. K., Smigel, M. D., and Gilman, A. G. (1982) *J. Biol. Chem. 257*, 11416−11423.
49. Wüthrich, K., Billeter, M., and Braun, W. (1983) *J. Mol. Biol. 169*, 949−961.
50. Clore, G. M., Gronenborn, A. M., Nilges, M., and Ryan, C. A. (1987) *Biochemistry 26*, 8012−8023.
51. Brünger, A. T. (1993) *X-PLOR Manual, Version 3.1*, Yale University, New Haven, CT.
52. Ramachandran, G. N., Ramakrishnan, C., and Sasisekharan, V. (1963) *J. Mol. Biol. 7*, 95−99.
53. Hyberts, S. G., Goldberg, M. S., Havel, T. F., and Wagner, G. (1992) *Protein Sci. 1*, 736−751.
54. Brooks, B. R., Bruccoleri, R. E., Olafson, B. D., States, D. J., Swaminathan, S., and Karplus, M. (1983) *J. Comput. Chem. 4*, 187−217.
55. Carpenter, K. A., and Ni, F. (1992) *J. Magn. Reson. 99*, 192−197.
56. Wang, Z., Jones, J. D., Rizo, J., and Gierasch, L. M. (1993) *Biochemistry 32*, 13991−13999.
57. Wong, S. K.-F., Parker, E. M., and Ross, E. M. (1990) *J. Biol. Chem. 265*, 6219−6244.
58. Savarese, T. M., and Fraser, C. M. (1992) *Biochem. J. 283*, 1−19.
59. Taylor, J. M., and Neubig, R. R. (1994) *Cell. Signalling 6*, 841−849.
60. Liu, J., Conklin, B. R., Blin, N., Yun, J., and Wess, J. (1995) *Proc. Natl. Acad. Sci. U.S.A. 92*, 11642−11646.
61. Liu, J., Blin, N., Conklin, B. R., and Wess, J. (1996) *J. Biol. Chem. 271*, 6172−6178.
62. Kostenis, E., Conklin, B. R., and Wess, J. (1997) *Biochemistry 36*, 1487−1495.
63. Strader, C. D., Sigal, I. S., and Dixon, R. A. F. (1989) *FASEB J. 3*, 1825−1832.
64. Blin, N., Yun, J., and Wess, J. (1995) *J. Biol. Chem. 270*, 17741−17748.
65. Weingarten, R., Ransnäs, L., Mueller, H., Sklar, L. A., and Bokoch, G. M. (1990) *J. Biol. Chem. 265*, 11044−11049.
66. Ferrin, T. E., Huang, C. C., and Jarvis, L. E. (1988) *J. Mol. Graphics 6*, 13−27.
67. Nicholls, A., Sharp, K. A., and Honig, B. (1991) *Proteins: Struct., Funct., Genet. 11*, 281−296.
68. Kohno, T., Kusunoki, H., Sato, K., and Wakamatsu, K. (1998) *J. Biomol. NMR* (in press).

BI972756P